AMSR-MODIS Marine Boundary Layer Water Vapor

Algorithm Theoretical Basis Document

Luis Millán, Matthew Lebsock, and Joao Teixeira

Version 1.0
September 2017

Jet Propulsion Laboratory California Institute of Technology Pasadena, California 91109-8099

Contents

1 Introduction **3**
- 1.1 Purpose of this Document . . . 3
- 1.2 Comments . . . 3

2 Overview of AMSR and MODIS **4**
- 2.1 AMSR . . . 4
- 2.2 MODIS . . . 4
- 2.3 Collocation . . . 5

3 Algorithm **6**
- 3.1 Methodology . . . 6
- 3.2 Binning algorithm . . . 7
- 3.3 Algorithm Inputs . . . 8
- 3.4 Algorithm Summary . . . 8

4 Output Data **9**
- 4.1 Data Characteristics . . . 10
- 4.2 Data Screening . . . 10

1 Introduction

Despite the importance of the marine boundary layer, it is not well represented in weather and climate models (e.g. Wyant et al., 2006). The problems representing boundary layer processes arise because most of its processes occur at scales smaller than the modeled grid, therefore, they need to be parametrized to represent its statistical properties. However, accurate parameterization of boundary layer processes, is still an unresolved challenge in weather and climate modeling (e.g. Teixeira et al., 2008). Part of the reason is the lack of measurements guiding the parameterizations development.

This document describes the synergy of collocated microwave radiometry and near-infrared imagery to estimate the marine boundary layer water vapor beneath uniform cloud fields. Microwave radiometry provides the total column water vapor, while the near-infrared imagery provides the water vapor above the cloud layers. The difference between the two gives the vapor between the surface and the cloud top, which may be interpreted as the boundary layer water vapor. In particular, we use data from the Advanced Microwave Scanning Radiometer (AMSR) as well as from the MOderate Resolution Imaging Spectroradiometer (MODIS). However, note that this technique could be applied to any combination of microwave and near infrared imagery that is capable of retrieving water vapor and spatially and temporally collocated. In combining the two datasets, we apply several flags as well as proximity tests to remove pixels with high clouds and/or intrapixel heterogeneity. The multi-sensor nature of the analysis demonstrates that there exists more information on boundary layer water vapor structure in the satellite observing system than is commonly assumed when considering the capabilities of single instruments.

1.1 Purpose of this Document

This document describes the theoretical basis of the AMSR-MODIS boundary layer water vapor algorithm to be used in the routine processing of data from AMSR-E and AMSR2 as well as from the MODIS instruments. The task of the algorithm is to merge the AMSR total column water vapor (CWV) with the MODIS partial CWV above the clouds into estimates of the boundary layer CWV (BL-CWV).

1.2 Comments

Initial release

2 Overview of AMSR and MODIS

This section gives an overview the input data used in the production of the AMSR-MODIS BL-CWV data. More details can be found elsewhere.

2.1 AMSR

AMSR, on board the JAXA's ADEOS-II and NASA's Aqua and AMSR2 on board JAXA's GCOM-W1 spacecrafts, is a conically scanning microwave radiometer measuring radiation at frequencies in the range 6.9–89 GHz. It provides day and night estimates of total CWV over the oceans by measuring near to the 22 GHz water vapor band. The native footprint of these estimates is 24 km. These CWV estimates have an estimated error of $\sim$0.6 mm (Wentz and Meissner, 2000), which we assume throughout this paper. The AMSR-E CWV retrievals have been inter-compared with retrievals from the Special Sensor Microwave Imager (SSM/I) instruments and from the Tropical Rainfall Measuring Mission (TRMM) microwave imager (TMI): overall, good agreement was found with systematic errors on the order of 0.1 to 0.2 mm (Wentz et al., 2005). A key feature of the AMSR measurements is its lack of sensitivity to non-precipitating clouds, therefore providing nearly uninterrupted measurements of this parameter over the oceans. Here we use Remote Sensing Systems (REMSS) CWV (version 7) which aggregates these estimates to a quarter degree spatial resolution.

2.2 MODIS

MODIS, on board NASA's Terra and Aqua satellites, has 36 visible, near-infrared and infrared spectral channels ranging from 0.4 to 14.4 μm which scans up to $\pm 55^o$ off nadir view. MODIS estimates CWV using two algorithms: one using infrared channels and another one using near-infrared channels. Here we use the Aqua MODIS (version 6) CWV estimates (MODIS product MYD05) retrieved using near-infrared solar radiation reflected by land surfaces, oceanic areas with sun glint or clouds at 1 km spatial resolution. This algorithm uses the ratio between the channels located in the 0.94μm water vapor band and adjacent window channels at 0.865 and 1.24μm to remove the effects of the variation of the surface reflectance with wavelength. Typical errors for these water vapor columns are estimated to be between 5% and 10% (Gao and Kaufman, 2003). MODIS CWV estimates over land were validated against the upward looking microwave radiometer located at the Southern Great Plains in Oklahoma, USA; overall, these data sets agreed within the expected errors (Gao and Kaufman, 2003).

To identify MODIS measurements above boundary layer clouds we apply several tests to filter out other conditions. First, we only used pixels identified by the MODIS algorithm as confident cloudy (MYD05 cloud mask). Second, we remove pixels where cirrus or aerosols were detected using the 1.38μm high cloud flag (MYD35). To remove partially partially cloud covered pixels, we exclude any pixel that is not surrounded by cloudy pixels, ensuring that we do not accept the edges of horizontally extensive cloud layers. Lastly, we used the differences in cloud top information (MYD06) between adjacent pixels to find homogeneous cloud fields. Note that in version 6, MODIS cloud top properties went through refinements involving an improved characterization of the MODIS spectral response functions for the 15 μm CO_2 bands and repeated comparisons with the cloud products of the Cloud Aerosol Lidar with Orthogonal Polarization (CALIOP) instrument onboard the CALIPSO platform. While in previous versions cloud top properties were provided only at 5 km spatial resolution, version 6 provides them at 1 km. Furthermore, cloud top height biases for boundary layer water clouds were reduced from

424 m to 197 m (Baum et al., 2012). This corresponds to an error of approximately 20 hPa for cloud top pressure, which we assume throughout this paper.

2.3 Collocation

MODIS, AMSR-E and AMSR2 are all part of the afternoon train (A-Train), a satellite constellation of several Earth observing satellites that fly in formation sampling the same volume of air within minutes of each other L'Ecuyer and Jiang (2010).

3 Algorithm

The basis for this algorithm has been outlined in Millán et al. (2016). This section reviews the details outlined in that study.

3.1 Methodology

BL-CWV, or more precisely, CWV below the cloud tops, is found by

$$W_{BL} = W_T - W_C \tag{1}$$

where W_T is the AMSR total CWV and W_C is the MODIS CWV above the clouds.

The majority of the algorithm consists on implementing a set of filtering criteria:

- Use MODIS pixels identified by the MYD05 cloud mask as confident cloudy
- Use MODIS pixels identified by the MYD35 cloud mask as free of high clouds
- Use MODIS pixels surrounded by pixels with the same flag characteristics (to eliminate pixels which might be partially cloud covered)
- Use MODIS pixels surrounded by pixels having the same cloud top height (to discard pixels with a high cloud heterogeneity)

After we have identified the MODIS pixels useful for this application, we geo-collocate the filtered MODIS pixels with the AMSR measurements which due to their different resolutions implies that many MODIS pixels used the same AMSR measurement. Figure 1 shows the scatter between AMSR-MODIS and radiosondes BL-CWV considering only AMSR-MODIS pixels in a 1 km radius from the radiosonde location, as well as considering only those radiosondes within six hours of the AMSR-MODIS local time measurements (13:45 pm) while applying the different filtering criteria.

To compute the BL-CWV from the radiosonde data we first identified the boundary layer height and then we integrate the specific humidity profile from that height to the surface. To find the boundary layer height we used three different methods: the location of the minimum vertical gradient of relative humidity, the location of the minimum vertical gradient of specific humidity, and the location of the maximum vertical gradient of potential temperature. Furthermore, we only use robust inversions, defined as those where the boundary layer height estimates of the 3 methods agree within 200 m. Once we know the mean boundary layer height, we compute the integrated water vapor from this height to the surface. The boundary layer heights estimated by each method are then used to compute an uncertainty in the radiosondes.

As shown in Figure 1, as we apply additional filtering conditions, the fit to the observed radiosondes data improves, and the correlation coefficient increases significantly. Using all the filtering criteria (panel D), the best fit line has a slope of 0.75, a very small offset (-0.04 cm) and an RMS deviation and bias of 0.49 and 0.3 cm, respectively; suggesting a good agreement between the two data sets.

Errors in these BL-CWV estimates are a combination (summing in quadrature) of the AMSR total CWV (0.6 mm) and the MODIS CWV above the clouds (always assumed to be 10%, the upper boundary given by Gao and Kaufman (2003)) errors.

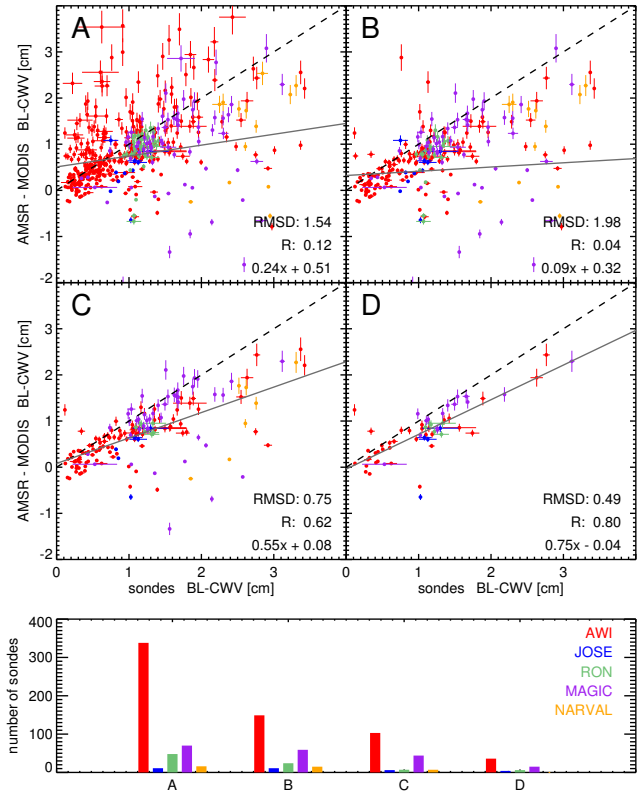

Figure 1: Scatter of AMSR-MODIS vs radiosondes boundary layer water vapor using four different filtering criteria: (A) Using all the MODIS points identified as cloudy (MYD05 cloud mask), (B) plus those free of high clouds (MYD35 cloud mask), (C) plus surrounded by pixels identified as cloudy and free of high clouds, (D) plus surrounded by pixels having the same cloud top pressure (MYD06 product). The dash black line is the one-to-one line. The gray line is the best fit line which equation is also given. Also, the linear Pearson correlation coefficient, R, is shown. The radiosondes errors (horizontal error bars) are computed from the differences between the boundary layer inversion height estimates calculated using the three different methods. Errors in the AMSR-MODIS BL-CWV estimates (vertical error bars) are a combination (summing in quadrature) of the AMSR total CWV and the MODIS CWV above the clouds errors.

3.2 Binning algorithm

After computing the AMSR-MODIS BL-CWV in the native MODIS CWV footprint, we aggregate measurements into a 1 by 1 degree grid in a daily or monthly granularity. Diagnostics saved for each grid cell are:

- Counts: Number of points in each grid cell
- Maximum: Maximum value in each grid cell
- Minimum: Minimum value in each grid cell
- Value: Average value in each grid cell

- Standard deviation: Standard deviation in each grid cell

Note that the monthly zonal means are obtained also by aggregating the AMSR-MODIS BL-CWV estimates rather than by simply averaging the daily files for that month.

3.3 Algorithm Inputs

The algorithm ingests inputs from MODIS and AMSR. Table 1 lists these inputs.

Table 1: Input variables to the AMSR-MODIS algorithm

Instrument	File type	description/variables
MODIS	MYD03	Geolocation fields (geodetic latitude and longitude)
MODIS	MYD05	Near infrared water vapor
MODIS	MYD06	Cloud top information (pressure, height, temperature)
MODIS	MYD35	Cloud mask
AMSR-E	Daily REMSS[a]	CWV (from 2002 to 2011)
AMSR2	Daily REMSS	CWV (2012 onwards)

[a] REMote Sensing Systems.

3.4 Algorithm Summary

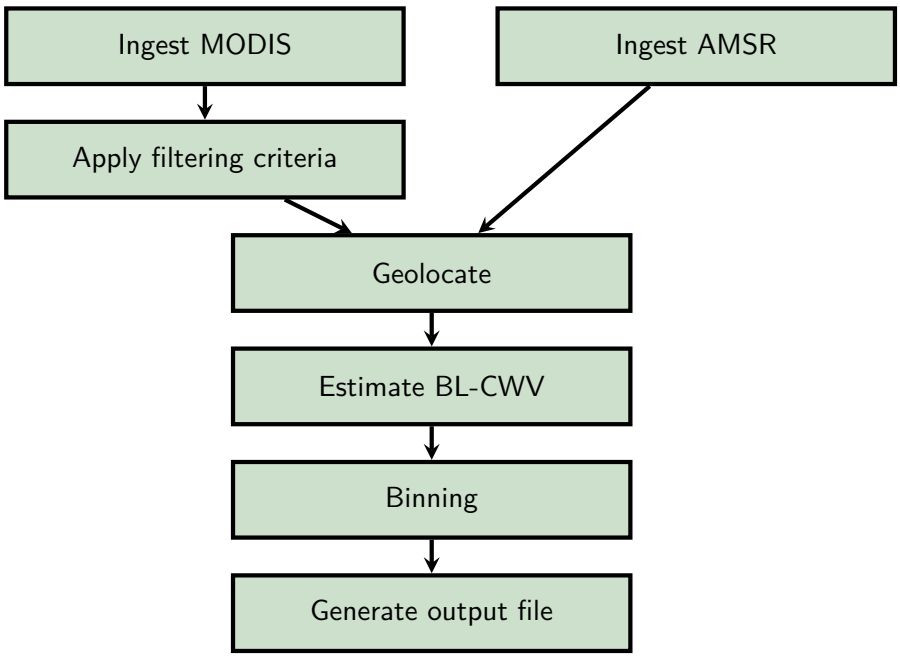

Figure 2: AMSR-MODIS BL-CWV algorithm flowchart

4 Output Data

The data is stored in the netcdf version 4 on a one-day or monthly granularity and named according to

`BLWV_D_V02.01_YYYYdDOY.nc4`

`BLWV_M_V02.01_YYYYdMM.nc4`

where <YYYY>, <MM> and <DOY> are the calendar year, month and the 3 digit day of they year, respectively.

Each file contains six swaths:

BL_CTH:	Boundary Layer Cloud Top Height	[Km]
BL_CTP:	Boundary Layer Cloud Top Pressure	[hPa]
BL_CTT:	Boundary Layer Cloud Top Temperature	[K]
BL_CWV:	Boundary Layer Column Water Vapor	[cm]
SST:	Sea Surface Temperature	[K]
Total_CWV:	Total Column Water Vapor	[cm]

Each swath contains the following geolocation fields:

EndDate	End date
Lat	Latitude
Lon	Longitude
StartDate	Start Date
Time	Time

as well the fields:

Counts	Number of points in each bin
Value	Average value in each grid cell
maximum	Maximum value in each grid cell
minimum	Minimum value in each grid cell
std_dev	Standard deviation in each grid cell

The units, longname and fill values are given in each field attributes called “unit”, “long_name”, and “_FillValue”.

4.1 Data Characteristics

Data is only available over the oceans.

The data is mapped to a 1 degree grid.

Note that the daily an monthly fields are derived from daytime only observations corresponding to the sampling time of the A-Train constellation with a fixed 1:30 PM equator crossing time. Therefore, they are not diurnal averages which we may expect to be different due to the subtle diurnal variations of the boundary layer height.

4.2 Data Screening

Bad value points are set to -999.99 and should be avoided.

Many negative values for BL-CWV are found in this dataset. These values need to be included in any data averaging to avoid high biases.

Acknowledgment

This work was performed under the MEaSUREs (2012) grant: "A Data Record of the Cloudy Boundary Layer".

References

B. A. Baum, W. P. Menzel, R. A. Frey, D. C. Tobin, R. E. Holz, S. A. Ackerman, A. K. Heidinger, and P. Yang. MODIS cloud-top property refinements for collection 6. *Journal of Applied Meteorology and Climatology*, 51(6):1145–1163, jun 2012. doi: 10.1175/jamc-d-11-0203.1.

B.-C. Gao and Y. J. Kaufman. Water vapor retrievals using moderate resolution imaging spectroradiometer (MODIS) near-infrared channels. *Journal of Geophysical Research: Atmospheres*, 108(D13), 2003. doi: 10.1029/2002jd003023.

T. S. L'Ecuyer and J. H. Jiang. Touring the atmosphere aboard the a-train. *Physics Today*, 63(7): 36–41, jul 2010. doi: 10.1063/1.3463626. URL https://doi.org/10.1063/1.3463626.

L. Millán, M. Lebsock, E. Fishbein, P. Kalmus, and J. Teixeira. Quantifying marine boundary layer water vapor beneath low clouds with near-infrared and microwave imagery. *Journal of Applied Meteorology and Climatology*, 55(1):213–225, jan 2016. doi: 10.1175/jamc-d-15-0143.1.

J. Teixeira, B. Stevens, C. S. Bretherton, R. Cederwall, S. A. Klein, J. K. Lundquist, J. D. Doyle, J. C. Golaz, A. A. M. Holtslag, D. A. Randall, A. P. Siebesma, and P. M. M. Soares. Parameterization of the atmospheric boundary layer: A view from just above the inversion. *Bulletin of the American Meteorological Society*, 89(4):453–458, apr 2008. doi: 10.1175/bams-89-4-453.

F. J. Wentz and T. Meissner. Amsr ocean algorithm, version 2. *Remote Sensing Systems*, 2000.

F. J. Wentz, C. Gentemann, and P. Ashcroft. Three years of ocean products from amsr-e: Evaluation and applications. *Int. Geosci. Remote. Se.*, pages 4929–4932, 2005.

M. C. Wyant, C. S. Bretherton, J. T. Bacmeister, J. T. Kiehl, I. M. Held, M. Zhao, S. A. Klein, and B. J. Soden. A comparison of low-latitude cloud properties and their response to climate change in three AGCMs sorted into regimes using mid-tropospheric vertical velocity. *Climate Dynamics*, 27(2-3):261–279, may 2006. doi: 10.1007/s00382-006-0138-4. URL https://doi.org/10.1007/s00382-006-0138-4.